

Role of nonlocal heat transport on the laser ablative Rayleigh–Taylor instability

Z. H. Chen,¹ X. H. Yang,^{1,2, a)} G. B. Zhang,¹ Y. Y. Ma,^{2,3} R. Yan,^{2,4} H. Xu,^{1,2} Z. M. Sheng,^{2,5} F. Q. Shao,¹ and J. Zhang^{2,5, b)}

¹⁾ College of Science, National University of Defense Technology, 410073 Changsha, China

²⁾ Collaborative Innovation Centre of IFSA, Shanghai Jiao Tong University, 200240 Shanghai, China

³⁾ College of Advanced Interdisciplinary Studies, National University of Defense Technology, 410073 Changsha, China

⁴⁾ Department of Modern Mechanics, University of Science and Technology of China, 230026 Hefei, China

⁵⁾ Key Laboratory for Laser Plasmas (Ministry of Education), School of Physics and Astronomy, Shanghai Jiao Tong University, 200240 Shanghai, China

Ablative Rayleigh-Taylor instability (ARTI) and nonlocal heat transport are the critical problems in laser-driven inertial confinement fusion, while their coupling with each other is not completely understood yet. Here the ARTI in the presence of nonlocal heat transport is studied self-consistently for the first time theoretically and by using radiation hydrodynamic simulations. It is found that the nonlocal heat flux generated by the hot electron transport tends to attenuate the growth of instability, especially for short wavelength perturbations. A linear theory of the ARTI coupled with the nonlocal heat flux is developed, and a prominent stabilization of the ablation front via the nonlocal heat flux is found, in good agreement with numerical simulations. This effect becomes more significant as the laser intensity increases. Our results should have important references for the target designing for inertial confinement fusion.

I. INTRODUCTION

The electron thermal conduction is a key process in inertial confinement fusion (ICF) as it largely determines the implosion energy and the hydrodynamic instabilities on the ablation front. The classical Spitzer-Härm (SH) thermal conduction model becomes inadequate when the electron mean free path λ_{ei} fails to meet the condition of being significantly smaller than the temperature gradient scale length $L_T = |T/\nabla T|$, i.e., $\lambda_{ei}/L_T \geq 0.01$, where T is the temperature^{1–6}. The energy transport of electrons will be nonlocal, which will both limit the heat flux and preheat the interior of the ablation front. Heat flux inhibition has an impact on various aspects, including the corona temperature, laser energy absorption, ablation rate, ablation pressure, conduction zone length, and shock amplitude. On the other hand, the preheating leads to higher entropy and reduced compression in the unablated region. Additionally, it enhances the mass ablation rate while flattening the ablation front. It may have an important impact on the ablative Rayleigh-Taylor instability (ARTI). Up to now, the effects of electron nonlocal transport on the stability and symmetry of the ablation front have not yet been well-understood.

When the energy from laser irradiation or X-rays is absorbed by the shell for direct drive or indirect drive ICF, extensive ablation of the outer surface of the shell develops. From the perspective of the ablation front's

reference frame, the ablation plasma accelerates the dense shell, ultimately giving rise to the occurrence of ARTI^{7–17}. It is well known that the mass ablation leads to a reduction in the ARTI growth rate and provides complete stabilization for the perturbations with wavelengths shorter than a cutoff wavelength λ_{cut} . The linear growth rate of the ARTI can be well approximately by the modified Takabe's formula¹⁸, $\gamma = \alpha \sqrt{kg/(1 + kL_m)} - \beta kV_a$, where α and β are dimensionless constants depending on ablator materials, k is the perturbation wavenumber, L_m is the minimum density gradient scale length, g is the acceleration, and V_a is the ablation velocity. Further, the analytical solution for perturbed growth has been cleverly obtained by asymptotic matching techniques¹⁹ and the WKB methods^{20–22}. It was found that the stabilizing mechanisms are attributed to vorticity convection^{8,9} and dynamical overpressure^{23,24}. It has been demonstrated through both simulations and experiments that the actual ARTI growth rates can be lower than predicted by the theories^{25–32}. This is usually attributed to the fact that the nonlocal effect can increase V_a and L_m via preheating, thus effectively suppressing the growth of the perturbation. The trend and cutoff wavelength of the growth rate curve can be roughly predicted using increasing V_a and L_m . However, there is still a significant gap exists between the predicted growth rates and the experimental observations^{30,31}. This indicates that our comprehension of the impacts of electron nonlocal transport on ARTI, along with any potential stabilizing mechanisms, remains incomplete. There is not any theory so far on the ARTI growths with the electron nonlocal transport taken into account.

In this paper, we investigate the ARTI in planar laser-

^{a)} xhyang@nudt.edu.cn

^{b)} jzhang1@sjtu.edu.cn

ablated foils with nonlocal heat transport considered self-consistently for the first time, where a nonlocal electron transport model known as the SNB model³³ is applied. It is shown that the growth rate, when considering the local heat flux, aligns well with predictions from by the classical ARTI theory. However, if assuming that non-local effects increase V_a and L_m only, the theory fails to fully explain the stabilization of ARTI by the nonlocal transport found in the simulation. A linear theory coupling with the nonlocal heat flux is proposed, which is in good agreement with simulations. The observation highlights that the nonlocal heat flux exerts a more pronounced inhibitory effect on perturbations with shorter wavelengths, leading to an increase in the cutoff wavelength.

II. RESULTS AND DISCUSSIONS

A. Numerical Simulations

We have performed simulations of a single-mode ARTI by using the radiation hydrodynamic code FLASH, in which different heat conduction models can be taken, such as the SH model or the SNB model^{34,35}. A planar CH foil is irradiated by a 2ω square-wave laser with peak intensity 4×10^{14} W/cm² and pulse duration 2 ns. Initial cosine perturbations of 10 μ m wavelength with an initial amplitude of 0.5 μ m are set on the leading surface of the planar CH foil. The thickness of the target is 40 μ m. Under the irradiation of the laser on the left side, the target starts to accelerate with an average acceleration $g^{SNB} = 148.06$ μ m/ns² and an average ablation velocity $V_a^{SNB} = 3.34$ μ m/ns when the SNB model is included. Figures 1(a) and 1(b) show the corresponding density profiles at time $t = 0.8$ ns and 1.5 ns, respectively. The presence of transverse heat flux within the dense target is evident as a result of hot electron preheating. It increases the entropy of the target, decreases the compressive density and increases the ablation rate, thus inhibiting the growth of ARTI. The peak-to-valley heights at the two moments are $h_1^{SNB} = 1.56$ μ m and $h_2^{SNB} = 6.72$ μ m, respectively. As a comparison, we have performed simulation with the classical SH heat conduction model under the same laser and target conditions. As shown in Figs. 1(c) and 1(d), the target moves with a higher average acceleration $g^{SH} = 150.44$ μ m/ns² and a lower average ablation velocity $V_a^{SH} = 2.69$ μ m/ns. The differences of the target acceleration are due to the slightly higher laser energy absorption of the SH model compared to the SNB model. In the meanwhile, the peak-to-valley heights obtained with the SH model at both moments are given by $h_1^{SH} = 2.19$ μ m and $h_2^{SH} = 10.47$ μ m, respectively, larger than that with the SNB model.

Figure 2(a) shows the perturbation amplitude evolution in both cases, where a similar evolution in the Richtmyer–Meshkov instability (RMI) phase before $t = 0.7$ ns are shown due to the similar laser energy absorption

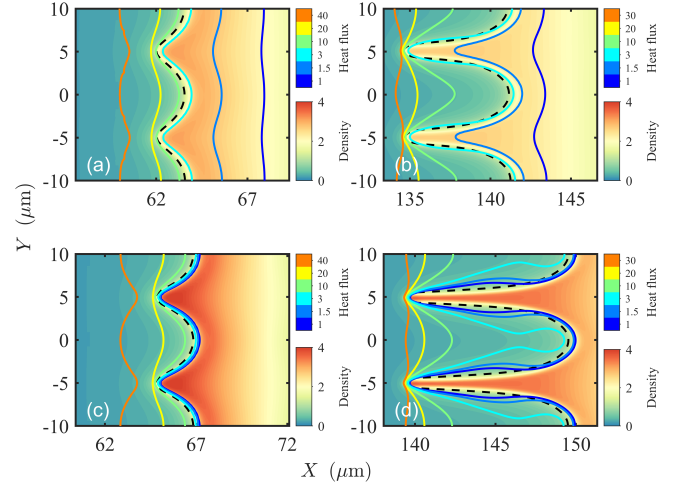


FIG. 1. The density profiles obtained with the SNB model [(a) and (b)] and the SH model [(c) and (d)] at time $t = 1$ ns [(a) and (c)] and $t = 1.5$ ns [(b) and (d)], where the density is in unit of g/cm³, the black dashed line signifies the ablation front and the irradiation originates from the left side. The transverse heat flux contours are overlaid on the density profiles in units of 10^{12} W/cm².

rate. The target starts to accelerate and the perturbation enters the RTI phase after 0.7 ns. During the linear phase, which spans from 0.8 ns to amplitudes reaching $0.1 \sim 0.2\lambda$, the growth rates for SNB and SH are $\gamma_{SNB}^{sim} = 4.20$ ns⁻¹ and $\gamma_{SH}^{sim} = 5.63$ ns⁻¹, respectively, where λ is the perturbation wavelength. The profiles of density and transverse heat flux at the perturbation peak along the acceleration direction are presented in Fig. 2(b). The SNB model with preheating gives a lower peak density and larger ablation front characteristic length. Table I lists the linear growth rates derived from the simulations and predicted by Kull's theory³⁶, as well as the relevant parameters determining the growth rates. The Kull's theory, henceforth called the classical theory, correctly predicts the linear growth rate for the classical SH model. However, it overestimates the growth rate even though that we apply the enhanced V_a and L_m from the nonlocal simulations. This suggests that a cautious approach should be taken when handling the hydrodynamic instability under the effects of nonlocal transport of electrons, as it cannot be adequately addressed solely by increasing V_a and L_m .

B. Development of the Nonlocal Linear Theory

To accurately predict the linear growth rate of ARTI, we have developed a linear theory that incorporates the nonlocal heat flux. Due to the complexity of the nonlocal multigroup diffusion equation, it is difficult to obtain an analytical solution for the ARTI growth rate. Therefore, this theory is based on the sharp boundary model (SBM)^{37,38}, following the numerical approach akin

TABLE I. Linear ARTI growth rate parameters for direct-drive planar CH targets determined from FLASH simulations, where $R = \rho_h/\rho_l$ is the density ratio of heavy to light fluid, $L_0 = L_m \nu^\nu/(\nu+1)^{\nu+1}$ is the characteristic thickness of the ablation front, ν is the power index for thermal conduction, γ_{sim} is the growth rate obtained by fitting the perturbation amplitude in the simulation, and γ_{th} is the growth rate predicted from the theory³⁶.

	V_a ($\mu\text{m}/\text{ns}$)	g ($\mu\text{m}/\text{ns}^2$)	L_0 (μm)	R	γ_{sim} (μm^{-1})	γ_{th} (μm^{-1})
SNB	3.3670	148.06	0.0497	3.8846	4.20	4.99
SH	2.6893	150.44	0.0369	4.2926	5.63	5.77

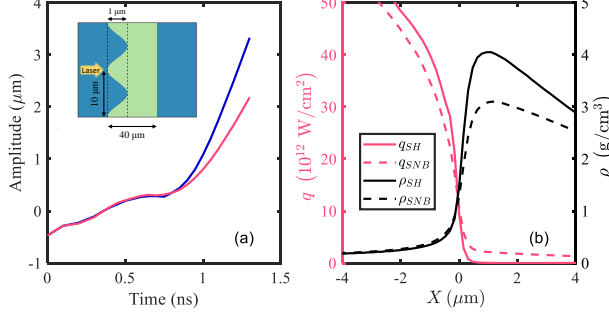


FIG. 2. (a) The evolution of perturbation amplitude over time reveals a phase reversal occurring at approximately 0.4 ns. The inset shows the initial setup. (b) The profiles of heat flux and density around the perturbation peak along the acceleration direction at 1.0 ns, with both models having their ablation fronts moved to $X = 0$.

to that employed by Kull et al.³⁶. Utilizing the nonlocal multigroup diffusion equation proposed by Schurtz et al.³³, the energy equation can be written as $\nabla \cdot (\mathbf{v} + \mathbf{Q}/(c_p \rho T)) = 0$ with the quasi-isobaric approximation, where \mathbf{v} (v_x, v_y) is the fluid velocity, ρ is the density, T is the temperature, c_p is the specific heat capacity under constant pressure, $\mathbf{Q} = -\kappa \nabla T - \sum_g \lambda_g \nabla H_g/3$ is the total heat flux, κ is the thermal conductivity, λ_g is the group mean free path, and H_g is the solution to the multigroup diffusion equations³³. The detailed derivation process is shown in the Methods.

The parameter $\Lambda = k_{c1} \lambda_1$, initially introduced in the nonlocal linear theory, is related to the electron characteristic free path λ_1 and can be used to estimate the strength of the preheating, where $k_{c1} = g/v_1^2$, v_1 is the ablation velocity. Fig 3(a) shows the dimensionless growth rate $\gamma_N = \gamma/(k_{c1} v_1)$ for $\Lambda = 1, 20, 100$, $R = 4$, $S = 0.7$, and $\nu = 2.5$, where $K = k/k_{c1}$ is the dimensionless wavenumber, $S = k_{c1} \chi_1/v_1$ is the reciprocal of Froude number, R is the density ratio of the heavy fluid to the light fluid. This is analogous to increasing λ_1 while keeping the ablation velocity V_a , the characteristic length of the ablation front L_0 and the acceleration g unchanged. At $\Lambda = 1$, the nonlocal theory essentially replicates the findings of the classical theoretical results. The growth rate curve has a maximum and cuts off at large wavenumbers due to ablative effects. As Λ gradually increases, the cutoff wavenumber decreases. This

implies that the nonlocal heat flux constitutes one of the important stabilizing factors for ARTI. It exerts varying degrees of suppression on perturbations of different wavelengths, displaying greater effectiveness in dampening perturbations with larger wavenumbers. Figure 3(b) shows the growth rate from the nonlocal and classical theories for $R = 2, 4, 10$. As R increases, the growth rate curves have a higher peak and a larger cutoff wavenumber, underscoring the heightened influence of the nonlocal heat flux on the cutoff wavenumber.

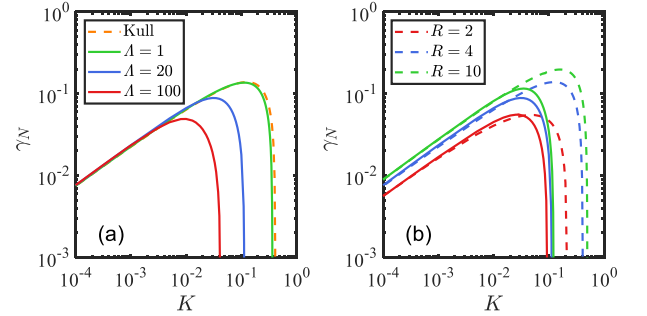


FIG. 3. (a) Growth rate curves for $\Lambda = 1, 20, 100$, $R = 4$, $S = 0.7$, and $\nu = 2.5$. (b) Growth rate curves for $R = 2, 4, 10$, $\Lambda = 20$, $S = 0.7$ and $\nu = 2.5$, where the solid line corresponds the nonlocal theory and the dashed line represents the classical theory.

Figure 4(a) shows the distribution of λ_{eff} for the case with a perturbation wavelength of $10 \mu\text{m}$ at $t = 1 \text{ ns}$, where $\lambda_{eff} = \sqrt{\lambda_a \lambda_b}$, $\lambda_a = \sum_g H_g / \left(\sum_g H_g / \lambda_g \right)$ and $\lambda_b = \sum_g \lambda_g \nabla H_g / \sum_g \nabla H_g$. Along the direction of the perturbation peak, we obtain the one-dimensional profile of λ_{eff} , i.e., Fig. 4(b). It is worth noted that λ_{eff} exhibits a minimum value in proximity to the ablation front. The growth rate of the nonlocal theory, $\gamma_{th}^{nonlocal} = 4.22 \text{ ns}^{-1}$, is determined by inserting the average λ_1 observed during the linear phase into the nonlocal dispersion relation and λ_1 is taken as the value of λ_{eff} near the ablation front. The theoretical growth rate is in good agreement with the that of the simulation, i.e., $\gamma_{SNB} = 4.20 \text{ ns}^{-1}$. It is found that the variation of λ_{eff} is dominated by λ_a . For the dense compressed region, the contribution of \mathbf{Q}_{SH} is neglected and the value of λ_{eff} increases with increasing depth into the target. Since

$\lambda_a = \sum_g \lambda_g \nabla \cdot \mathbf{Q}_{SNB}^g / \nabla \cdot \mathbf{Q}_{SNB} (\nabla \cdot \mathbf{Q}_{SNB}^g = H_g / \lambda_g)$, a larger λ_{eff} indicates that the hot electrons contribute more to the change of energy. For the outer side of the ablation front, λ_{eff} also increases during the process away from the target. This phenomenon arises because \mathbf{Q}_{SNB} is significantly smaller than \mathbf{Q}_{SH} in this region, and the electron mean free path λ_{ei} gradually increases outward. Consequently, λ_{eff} serves as a gauge of the intensity of nonlocal effects within the ablation front.

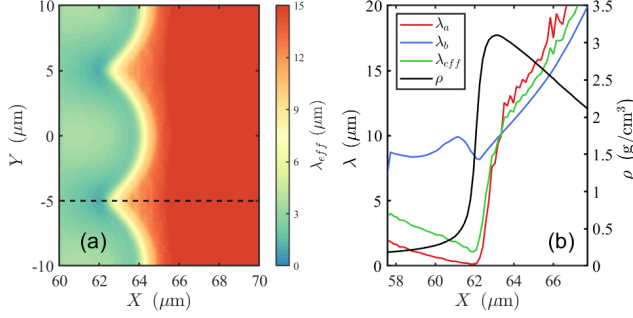


FIG. 4. (a) Spatial distribution of the effective free path λ_{eff} for a $10 \mu\text{m}$ perturbation wavelength at 1 ns. (b) Distribution of the effective free path λ_{eff} along the direction of the dashed line in (a).

To understand completely the effect of the nonlocal heat flux on the perturbations with different wavelengths, we have performed simulations with wavelengths of 8, 15, 20, and 30 μm , respectively. All other parameters are kept the same as that in the 10 μm case. The results are shown in Fig. 5(a). The simulations of the classical SH model are in good agreement with the classical ATRI theory at all perturbation wavelengths. For the SNB model, the simulations of the long wavelengths are consistent with the classical theory. However, for the short wavelength perturbations, the classical theory, even taking the relevant hydrodynamic parameters into account, deviates from the simulations, while our nonlocal theory agrees well with the simulations. This confirms that it is necessary to consider the nonlocal heat flux appropriately in the energy equation, which can increase the cutoff wavelength of the instability. As the laser intensity increases, both the nonlocal heat flux and the electron effective free path λ_{eff} increase, resulting in a more pronounced influence of the nonlocal effect on the growth of ARTI. We have studied the effect of the magnitude of the nonlocal heat flux on ARTI by using different laser intensities. The perturbation wavelength here is 10 μm , and other parameters remain unchanged. As shown in Fig. 5(b), λ_{eff} indeed increases as the laser intensity increases, and the classical theory gradually deviates from the simulations. This is in agreement with the experimental observations of Smalyuk et al.^{30,31}. It is seen that the theoretical model coupled with the nonlocal heat flux consists better with the simulations in all

intensity ranges.

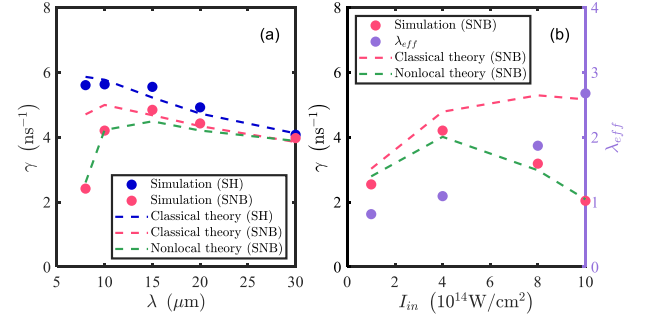


FIG. 5. (a) Linear growth rates of the ARTI with the two models, where the results for the classical and nonlocal theories are the growth rates obtained by substituting the hydrodynamic parameters from the simulations (SH or SNB model) into the classical and nonlocal dispersion relations, respectively. (b) Linear growth rates (left y axis) and electron effective free path λ_{eff} (right y axis) for different laser intensities. The peak laser intensities are set to 1, 4, 8 and $10 \times 10^{14} \text{W/cm}^2$, respectively.

III. CONCLUSIONS

In summary, we have conducted a pioneering study on the impact of nonlocal electron transport on ARTI, encompassing the comprehensive processes of laser heating and transport, within a laser-irradiated target. The nonlocal effects are crucial for laser driven ICF target design, and their stabilizing effect proves advantageous in mitigating the hydrodynamic instability growth within the target. The classical theory fails to predict the ARTI growth rate in short wavelength perturbations due to ignorance of the hot electron preheating. A linear theory coupled with nonlocal heat flux is developed, and it gives consistent results to numerical simulations. The nonlocal heat flux has different degrees of suppression on different perturbation wavelengths. This suppression effect is particularly efficient for short wavelength perturbations, meaning that the nonlocal thermal conduction increases the cutoff wavelength of the perturbation.

The electron effective free path λ_{eff} is related to the magnitude of the nonlocal heat flux and can serve as an indicator of the intensity of preheating. The results of the local linear theory applying increasing the ablation velocity and density gradient scale length gradually deviate from the simulation results when λ_{eff} increases, while the results of the nonlocal linear theory agree with the simulation results. The suppression of perturbations by nonlocal heat flux will be enhanced when λ_{eff} increases. The linear growth theory of ARTI and the influence of electron nonlocal transport on ARTI presented here should provide a important reference for laser and target design in laser fusion.

IV. METHODS

A. Simulation Method

The simulations in this work are carried out by using the hydrodynamics code FLASH³⁴, which includes capabilities for electron thermal conduction, laser energy deposition and multigroup radiative diffusion, and is widely used to carry out modelling of high energy density physics. We have extended the code to include electron nonlocal heat transport modelling capabilities. The classical heat conduction equation is

$$\rho c_v \frac{\partial T}{\partial t} = \nabla \cdot \kappa \nabla T, \quad (1)$$

where ρ is the mass density, c_v is the specific heat at constant volume, T is the temperature, κ is the thermal conductivity. The SNB model³³ introduces nonlocal heat flux, which modifies the heat conduction equation

$$\rho c_v \frac{\partial T}{\partial t} = \nabla \cdot \kappa \nabla T + \sum_g \frac{\lambda_g}{3} \nabla H_g, \quad (2)$$

where H_g is the solution of the multigroup diffusion equations,

$$\left(\frac{1}{\lambda_g} - \nabla \cdot \frac{\lambda_g}{3} \nabla \right) H_g = \nabla \cdot \eta_g \kappa \nabla T, \quad (3)$$

$\lambda_g = 2(E_{g-1/2}/k_B T)^2 \lambda_{ei}$ is the mean free path of electrons for different energy groups E_g , $E_{g-1/2} = (E_g + E_{g-1})/2$, k_B is the Boltzmann constant, λ_{ei} is the electron-ion mean free path, $\eta_g = \int_{E_{g-1}/k_B T}^{E_g/k_B T} \beta^4 e^{-\beta} d\beta / 24$. The HYPRE³⁹ linear algebra package is used to solve these diffusion equations.

In the simulations, we used an adaptive grid, and applied open and reflective boundary conditions in the x and y directions, respectively. The target uses QEOS parameters based on the Thomas-Fermi model⁴⁰. Due to the low Z value for the CH target, we turn off the radiation unit. The initial density of the CH target is 1.1 g/cm^3 , and the vacuum region is filled with helium of density 10^{-6} g/cm^3 . The initial temperature is uniformly set to 290 K.

B. Theoretical Method

The derivation of the ARTI linear growth rate coupling with the hot electron nonlocal transport is presented below. We consider a two-dimensional slab in the xy plane, with the gravitational acceleration g taken along the positive axis of y . According to the quasi-isobaric pressure model proposed by Kull et al.³⁶, the conservation equations for mass, momentum, and energy are given by

$$\frac{\partial \rho}{\partial t} + \nabla \cdot (\rho \mathbf{v}) = 0, \quad (4)$$

$$\rho \frac{\partial v_x}{\partial t} + \rho v_x \frac{\partial v_x}{\partial x} + \rho v_y \frac{\partial v_x}{\partial y} = -\frac{\partial p}{\partial x}, \quad (5)$$

$$\rho \frac{\partial v_y}{\partial t} + \rho v_x \frac{\partial v_y}{\partial x} + \rho v_y \frac{\partial v_y}{\partial y} = -\frac{\partial p}{\partial y} - \rho g, \quad (6)$$

$$\nabla \cdot \left(\mathbf{v} + \frac{\mathbf{Q}}{c_p \rho T} \right) = 0, \quad (7)$$

where ρ is the mass density, \mathbf{v} (v_x, v_y) is the fluid velocity, p is the pressure, \mathbf{Q} is the heat flux, T is the temperature, and c_p is the specific heat capacity under constant pressure. The nonlocal multigroup diffusion equation proposed by Schurtz et al.³³ is

$$\sum_g \frac{H_g}{\lambda_g} - \nabla \cdot \sum_g \frac{\lambda_g}{3} \nabla H_g = \nabla \cdot \kappa \nabla T, \quad (8)$$

where κ is the thermal conductivity, λ_g is the group mean free path, H_g is the solution to the multigroup diffusion equations and the total heat flux is $\mathbf{Q} = -\kappa \nabla T - \sum_g \lambda_g \nabla H_g / 3$. Defining $\lambda_a = \sum_g H_g / \left(\sum_g H_g / \lambda_g \right)$, $\lambda_b = \sum_g \lambda_g \nabla H_g / \sum_g \nabla H_g$ and $\lambda_{eff} = \sqrt{\lambda_a \lambda_b}$, Eq. (8) can be rewritten as

$$\frac{\sum_g H_g}{\lambda_a} - \nabla \cdot \frac{\lambda_b}{3} \nabla \sum_g H_g = \nabla \cdot \kappa \nabla T. \quad (9)$$

All variables are assumed of the form $X(x, y, t) = X_0 + \delta X(y) e^{\gamma t + i k x}$, where γ is the growth rate and k is the perturbation wavenumber. The linearization of Eqs. (4)-(7) for the perturbations $\delta X(y)$ gives

$$\gamma \delta \rho + i k \rho_0 \delta v_x + (\rho_0 \delta v_y + v_0 \delta \rho)' = 0, \quad (10)$$

$$\gamma \rho_0 \delta v_x + i k \delta p + \rho_0 v_0 \delta v_x' = 0, \quad (11)$$

$$\gamma(\rho_0 \delta v_y + v_0 \delta \rho) + i k \rho_0 v_0 \delta v_x - g \delta \rho + (2 \rho_0 v_0 \delta v_y + v_0^2 \delta \rho + \delta p)' = 0, \quad (12)$$

$$i k \delta v_x + (\delta v_y)' - \frac{1}{c_p \rho_0 T_0} \frac{\sum_g \delta H_g}{\lambda_a} = 0, \quad (13)$$

where the prime denotes differentiation with respect to y . The energy equation (13) is obtained by the following relation

$$\nabla \cdot \mathbf{Q} = -\frac{\sum_g H_g}{\lambda_a}. \quad (14)$$

The perturbation of the heat flux can be approximated as $\delta \mathbf{Q} = -\kappa \nabla (\delta T) - \lambda_b \nabla \left(\delta \sum_g H_g \right) / 3$. Defining the thermal diffusivity coefficient $\chi = \kappa / (\rho c_p)$ and the nonlocal

coefficient $\chi_n = \lambda_b / (3c_p \rho)$, for the constant pressure, the following relation holds

$$\frac{\delta Q}{c_p \rho T} = \chi \nabla \frac{\delta \rho}{\rho} - \chi_n \nabla \left(\frac{\delta \sum H_g}{T} \right). \quad (15)$$

Thus Eq. (13) can also be written as

$$ik\delta v_x - k^2 \chi \frac{\delta \rho}{\rho} + k^2 \chi_n \left(\frac{\delta \sum H_g}{T} \right) + \left[\delta v_y + \left(\chi \frac{\delta \rho}{\rho} \right)' + \left(\chi_n \frac{\delta \sum H_g}{T} \right)' \right]' = 0. \quad (16)$$

Taking the regions of $y < 0$ (region 1), $y = 0$, and $y > 0$ (region 2) denote heavy fluid, ablation front, and light fluid, respectively. For this sharp boundary, we integrate over the boundary to obtain the following jump conditions

$$\begin{aligned} \|\rho \delta v_y + v \delta \rho\| &= 0, \\ \|\delta v_x\| &= 0, \\ \|2\rho v \delta v_y + v^2 \delta \rho + \delta p\| &= 0, \\ \left\| \delta v_y + \left(\chi \frac{\delta \rho}{\rho} \right)' - \left(\chi_n \frac{\delta \sum H_g}{T} \right)' \right\| &= 0, \\ \left\| \chi \frac{\delta \rho}{\rho} \right\| &= 0, \\ \left\| \chi_n \frac{\delta \sum H_g}{T} \right\| &= 0, \end{aligned} \quad (17)$$

$\|X\| = X_1 - X_2$ denotes the jump of the variable X at the interface. The perturbations on both sides of the discontinuous interface are analyzed next. Assuming that the perturbations have the form $\delta X(y) \propto e^{ly}$, according to Eq. (9) we obtain the equation for $\delta \sum H_g$

$$\left[1 - \frac{\lambda_a \lambda_b}{3} (l^2 - k^2) \right] \frac{\delta \sum H_g}{\lambda_a} = \kappa (l^2 - k^2) \delta T. \quad (18)$$

Assuming that the coefficient of $\delta \sum H_g$ is not zero, the following relation holds

$$\frac{1}{c_p \rho T} \frac{\delta \sum H_g}{\lambda_a} = \frac{-\chi (l^2 - k^2)}{1 - \frac{\lambda_{eff}^2}{3} (l^2 - k^2)} \frac{\delta \rho}{\rho}. \quad (19)$$

The characteristic equation about $\delta \rho$ can be obtained from Eqs. (13) and (19), while the equation about δv_y can be obtained from Eqs. (10) and (12).

$$\left[\gamma + vl - \chi (l^2 - k^2) - (\gamma + vl) \frac{\lambda_{eff}^2}{3} (l^2 - k^2) \right] \delta \rho = 0, \quad (20)$$

$$(l^2 - k^2) (\gamma + vl) \rho \delta v_y + [l(\gamma + vl)^2 + gk^2] \delta \rho = 0. \quad (21)$$

Eq. (20) is a cubic equation with respect to l and is no longer a simple quadratic equation (Eq. 9(b) in Ref. 36). Define l_1 , l_2 and l_3 as solutions of Eq. (20), where $l_1 > 0 > l_2 > l_3$. For $y < 0$, the allowed modes are k , l_1 , and for $y > 0$, the allowed modes are $-k$, $-\gamma/v_2$, l_2 , l_3 , where the subscript 1 denotes region 1 and the subscripts 2 and 3 denote region 2. For the incompressible surface modes with $l = \pm k$, it can be deduced that

$$\begin{aligned} \delta v_y &= c_{1,2} e^{\pm ky}, \\ \delta v_x &= \pm i \delta v_y, \\ \delta p &= \mp (\rho/k) (\gamma \pm vk) \delta v_y, \\ \delta \rho &= 0, \end{aligned} \quad (22)$$

for the convection mode with $l = -\gamma/v_2$,

$$\begin{aligned} \delta v_y &= c_3 e^{-\gamma/v_2 y}, \\ \delta v_x &= -i\gamma/(kv) \delta v_y, \\ \delta p &= 0, \\ \delta \rho &= 0, \end{aligned} \quad (23)$$

and for the thermal conduction modes with $l = l_1, l_2, l_3$,

$$\begin{aligned} \frac{\delta \rho}{\rho_0} &= c_{4,5,6} e^{l_{1,2,3} y}, \\ \delta v_y &= \frac{l_{1,2,3} (\gamma + vl_{1,2,3})^2 + gk^2}{(k^2 - l_{1,2,3}^2) (\gamma + vl_{1,2,3})} \frac{\delta \rho}{\rho}, \\ \delta v_x &= i \frac{k (\gamma + vl_{1,2,3})^2 - kgl_{1,2,3}}{(k^2 - l_{1,2,3}^2) (\gamma + vl_{1,2,3})} \frac{\delta \rho}{\rho}, \\ \delta p &= (i/k) \rho (\gamma + vl_{1,2,3}) \delta v_x, \end{aligned} \quad (24)$$

where $c_1 \sim c_6$ are arbitrary coefficients. The six jump conditions form a linear system of six unknown mode amplitudes. For $y \rightarrow 0^-$, the allowed modes are k and l_1 , and the perturbation is denoted as

$$\begin{aligned} \delta v_y &= a + r_1 b, \\ \delta v_x &= ia + is_1 b, \\ \delta \rho &= \frac{\rho_1}{v_1} b, \\ \delta p &= -\frac{\rho_1 \gamma}{k} (1 + u_1) a - \frac{\gamma}{k} \rho_1 (1 + u_1 p_1) s_1 b. \end{aligned} \quad (25)$$

For $y \rightarrow 0^+$, the allowed modes are $-k$, $-\gamma/v_2$, l_2 and l_3 , and the perturbations are

$$\begin{aligned} \delta v_y &= c + d + r_2 e + r_3 f, \\ \delta v_x &= -ic - id/u_2 + is_2 e + is_3 f, \\ \delta \rho &= \frac{\rho_2}{v_2} e + \frac{\rho_2}{v_2} f, \\ \delta p &= \frac{\rho_2 \gamma}{k} (1 - u_2) c - \frac{\gamma}{k} \rho_2 (1 + u_2 p_2) s_2 e \\ &\quad - \frac{\gamma}{k} \rho_2 (1 + u_2 p_3) s_3 f, \end{aligned} \quad (26)$$

where $a \sim f$ are arbitrary constants, $u = kv/\gamma$, $p = l/k$,

$$r = \frac{l(\gamma + v_0 l)^2 + gk^2}{(k^2 - l^2) (\gamma + v_0 l) v}, \quad (27)$$

$$s = p(1 + r) + 1/u. \quad (28)$$

Inserting Eqs. (25) and (26) into the jump conditions (17) yields the following relations

$$\begin{aligned}
 R[a + (1 + r_1)b] &= [c + d + (1 + r_2)e + (1 + r_3)f], \\
 a + s_1b &= -c - \frac{d}{u_2} + s_2e + s_3f, \\
 \left(1 - \frac{1}{u_1}\right)a + t_1b &= \left(1 + \frac{1}{u_2}\right)c + 2d + t_2e + t_3f, \\
 a + r_1b + p_1h_1b &= c + d + r_2e + r_3f + p_2h_2e + p_3h_3f, \\
 z_1b &= z_2e + z_2f, \\
 x_1b &= x_2e + x_2f,
 \end{aligned} \tag{29}$$

where $R = \rho_1/\rho_2$ is the density ratio of the heavy fluid to the light fluid, $t = 1 + 2r - s(p + 1/u)$, $z = \chi k/v$, $x = k\gamma\lambda^2(1 + up)/(3v)$, $h = x + z$. We obtain the following matrix system

$$\mathbf{A} \cdot \mathbf{Y} = 0, \tag{30}$$

where \mathbf{A} is the coefficient matrix given by

$$\mathbf{A} = \begin{bmatrix} R & R(r_1 + 1) & -1 & -1 & -(r_2 + 1) & -(r_3 + 1) \\ 1 & s_1 & 1 & \frac{1}{u_2} & -s_2 & -s_3 \\ 1 - \frac{1}{u_1} & t_1 & -1 - \frac{1}{u_2} & -2 & -t_2 & -t_3 \\ 1 & r_1 + p_1h_1 & -1 & -1 & -(r_2 + p_2h_2) & -(r_3 + p_3h_3) \\ 0 & z_1 & 0 & 0 & -z_2 & -z_2 \\ 0 & x_1 & 0 & 0 & -x_2 & -x_3 \end{bmatrix}, \tag{31}$$

and \mathbf{Y} is a vector of undetermined coefficients given by

$$\mathbf{Y}^T = [a \ b \ c \ d \ e \ f]. \tag{32}$$

The dispersion relation with respect to γ can be derived by setting the determinant of the coefficient matrix \mathbf{A} equal to zero. Consistent with Ref. 36, the dimensionless wavenumber $K = k/k_{c1}$, the reciprocal of Froude number $S = k_{c1}\chi_1/v_1$, the dimensionless growth rate $\gamma_N = \gamma/(k_{c1}v_1)$ and the dimensionless free path $\Lambda = k_{c1}\lambda_1 = k_{c1}\lambda_2/R^3$ are introduced.

ACKNOWLEDGMENTS

This work was supported by the National Natural Science Foundation of China (Grant Nos. 12175309, 11975308, 12005297, and 12275356), the Strategic Priority Research Program of Chinese Academy of Science (Grant Nos. XDA25050200, XDA25050400, and XDA25010100), the Defense Industrial Technology Development Program (Grant. JCKYS2023212807). X.H.Y. also acknowledges the financial support from Fund for NUDT Young Innovator Awards (No. 20180104).

REFERENCE

- ¹Luciani, J. F., Mora, P. & Virmont, J. Nonlocal Heat Transport Due to Steep Temperature Gradients. *Physical Review Letters* **51**, 1664–1667 (1983).
- ²Bell, A. R. Non-Spitzer heat flow in a steadily ablating laser-produced plasma. *Physics of Fluids* **28**, 2007 (1985).
- ³Mora, P. & Luciani, J. Nonlocal electron transport in laser created plasmas. *Laser and Particle Beams* **12**, 387–400 (1994).
- ⁴Gregori, G. *et al.* Effect of Nonlocal Transport on Heat-Wave Propagation. *Physical Review Letters* **92**, 205006 (2004).
- ⁵Hench, R. J. *et al.* Observation of Nonlocal Heat Flux Using Thomson Scattering. *Physical Review Letters* **121**, 125001 (2018).
- ⁶Atzeni, S. *et al.* Shock ignition of thermonuclear fuel: Principles and modelling. *Nuclear Fusion* **54**, 054008 (2014).
- ⁷Bodner, S. E. Rayleigh-Taylor Instability and Laser-Pellet Fusion. *Physical Review Letters* **33**, 761–764 (1974).
- ⁸Kull, H. Theory of the Rayleigh-Taylor instability. *Physics Reports* **206**, 197–325 (1991).
- ⁹Kilkenny, J. D. *et al.* A review of the ablative stabilization of the Rayleigh-Taylor instability in regimes relevant to inertial confinement fusion. *Physics of Plasmas* **1**, 1379–1389 (1994).
- ¹⁰Piriz, A. R. & Portugues, R. F. Hydrodynamic instabilities in an ablation front. *Plasma Physics and Controlled Fusion* **46**, 935–950 (2004).
- ¹¹Betti, R. & Sanz, J. Bubble Acceleration in the Ablative Rayleigh-Taylor Instability. *Physical Review Letters* **97**, 205002 (2006).
- ¹²Betti, R. & Hurricane, O. A. Inertial-confinement fusion with lasers. *Nature Physics* **12**, 435–448 (2016).
- ¹³Zhou, Y. Rayleigh-Taylor and Richtmyer-Meshkov instability

- induced flow, turbulence, and mixing. I. *Physics Reports* **720**–**722**, 1–136 (2017).
- ¹⁴Zhang, F. *et al.* Enhanced energy coupling for indirect-drive fast-ignition fusion targets. *Nature Physics* **16**, 810–814 (2020).
 - ¹⁵Ramis, R., Canaud, B., Temporal, M., Garbett, W. J. & Philippe, F. Analysis of three-dimensional effects in laser driven thin-shell capsule implosions. *Matter and Radiation at Extremes* **4**, 055402 (2019).
 - ¹⁶Matsuo, K. *et al.* Enhancement of Ablative Rayleigh-Taylor Instability Growth by Thermal Conduction Suppression in a Magnetic Field. *Physical Review Letters* **127**, 165001 (2021).
 - ¹⁷Qiao, X. & Lan, K. Novel Target Designs to Mitigate Hydrodynamic Instabilities Growth in Inertial Confinement Fusion. *Physical Review Letters* **126**, 185001 (2021).
 - ¹⁸Betti, R., Goncharov, V. N., McCrory, R. L. & Verdon, C. P. Growth rates of the ablative Rayleigh-Taylor instability in inertial confinement fusion. *Physics of Plasmas* **5**, 1446–1454 (1998).
 - ¹⁹Sanz, J. Self-consistent Analytical Model of the Rayleigh-Taylor Instability in Inertial Confinement Fusion. *Physical Review Letters* **73**, 2700–2703 (1994).
 - ²⁰Goncharov, V. N., Betti, R., McCrory, R. L., Sorotokin, P. & Verdon, C. P. Self-consistent stability analysis of ablation fronts with large Froude numbers. *Physics of Plasmas* **3**, 1402–1414 (1996).
 - ²¹Goncharov, V. N., Betti, R., McCrory, R. L. & Verdon, C. P. Self-consistent stability analysis of ablation fronts with small Froude numbers. *Physics of Plasmas* **3**, 4665–4676 (1996).
 - ²²Betti, R., Goncharov, V. N., McCrory, R. L. & Verdon, C. P. Self-consistent cutoff wave number of the ablative Rayleigh-Taylor instability. *Physics of Plasmas* **2**, 3844–3851 (1995).
 - ²³Piriz, A. R., Sanz, J. & Ibañez, L. F. Rayleigh-Taylor instability of steady ablation fronts: The discontinuity model revisited. *Physics of Plasmas* **4**, 1117–1126 (1997).
 - ²⁴Goncharov, V. N. Theory of the Ablative Richtmyer-Meshkov Instability. *Physical Review Letters* **82**, 2091–2094 (1999).
 - ²⁵Shigemori, K. *et al.* Measurements of Rayleigh-Taylor Growth Rate of Planar Targets Irradiated Directly by Partially Coherent Light. *Physical Review Letters* **78**, 250–253 (1997).
 - ²⁶Azechi, H. *et al.* Direct-drive hydrodynamic instability experiments on the GEKKO XII laser. *Physics of Plasmas* **4**, 4079–4089 (1997).
 - ²⁷Glendinning, S. G. *et al.* Measurement of a Dispersion Curve for Linear-Regime Rayleigh-Taylor Growth Rates in Laser-Driven Planar Targets. *Physical Review Letters* **78**, 3318–3321 (1997).
 - ²⁸Honda, M. *et al.* Effects of non-local electron thermal transport on ablative Rayleigh-Taylor instability. *Fusion Engineering and Design* **44**, 205–208 (1999).
 - ²⁹Sakaiya, T. *et al.* Ablative Rayleigh-Taylor Instability at Short Wavelengths Observed with Moiré Interferometry. *Physical Review Letters* **88**, 145003 (2002).
 - ³⁰Smalyuk, V. A. *et al.* Rayleigh-Taylor Growth Stabilization in Direct-Drive Plastic Targets at Laser Intensities of $\sim 1 \times 10^{15}$ W/cm². *Physical Review Letters* **101**, 025002 (2008).
 - ³¹Smalyuk, V. A. *et al.* Systematic study of Rayleigh-Taylor growth in directly driven plastic targets in a laser-intensity range from $\sim 2 \times 10^{14}$ to $\sim 1.5 \times 10^{15}$ W/cm². *Physics of Plasmas* **15**, 082703 (2008).
 - ³²Li, J. *et al.* Mitigation of the ablative Rayleigh-Taylor instability by nonlocal electron heat transport. *Matter and Radiation at Extremes* **7**, 055902 (2022).
 - ³³Schurtz, G. P., Nicolai, Ph. D. & Busquet, M. A nonlocal electron conduction model for multidimensional radiation hydrodynamics codes. *Physics of Plasmas* **7**, 4238 (2000).
 - ³⁴Fryxell, B. *et al.* FLASH: An Adaptive Mesh Hydrodynamics Code for Modeling Astrophysical Thermonuclear Flashes. *The Astrophysical Journal Supplement Series* **131**, 273–334 (2000).
 - ³⁵Chen, Z. H. *et al.* Effect of non-local transport of hot electrons on the laser-target ablation. *Physics of Plasmas* **30**, 062710 (2023).
 - ³⁶Kull, H. J. & Anisimov, S. I. Ablative stabilization in the incompressible Rayleigh-Taylor instability. *Physics of Fluids* **29**, 2067 (1986).
 - ³⁷Piriz, A. R. Hydrodynamic instability of ablation fronts in inertial confinement fusion. *Physics of Plasmas* **8**, 997–1002 (2001).
 - ³⁸Sanz, J., Ramírez, J., Ramis, R., Betti, R. & Town, R. P. J. Non-linear Theory of the Ablative Rayleigh-Taylor Instability. *Physical Review Letters* **89**, 195002 (2002).
 - ³⁹hypre: High performance preconditioners. <https://llnl.gov/casc/hypre>, <https://github.com/hypre-space/hypre>.
 - ⁴⁰More, R. M., Warren, K. H., Young, D. A. & Zimmerman, G. B. A new quotidian equation of state (QEOS) for hot dense matter. *Physics of Fluids* **31**, 3059 (1988).